4. SYNTHESIS AND CHARACTERIZATION OF MESOPOROUS SILICA NANOPARTICLES

Table 4.1: List of Chemicals:

Sr. No.	Chemicals	Source and Place
1	Sodium silicate (Na_2SiO_3)	Gift sample by Arihant Chemical Works, India.
2	Cetyltrimethylammonium bromide (CTAB)	Himedia chemicals, India
3	Isopropyl alcohol (IPA)	Rankem, India
4	Ethyl acetate	Rankem, India
5	Copper chloride ($CuCl_2$)	Gift sample by Arihant Chemical Works, India.
6	Zinc chloride ($ZnCl_2$)	Gift sample by Arihant Chemical Works, India.
7	poly(ethylene-oxide)-block-poly(propylene-oxide)- block-poly(ethylene-oxide) (Poloxamer 407/pluronic F127)	BASF, India
8	Hydrochloric acid (HCl)	Rankem, India

Table 4.2: List of Equipments.

Sr. no.	Equipment	Company Name and Place
1	Digital weighing machine	Type AX 120,Shimadzu, Japan
2	Digital pH meter	Lab India instruments Ltd, India
3	Magnetic Stirrer	Remi equipment, India
4	Bath Sonicator	Fast clean ultra-cleaner, India
5	Hot air oven	Sedko laboratory equipments, India
6	Muffle furnace	Shreeji pharmaceutical scientific and laboratory equipments, India
7	UV visible spectrophotometer 1800	Shimadzu, Japan
8	Particle size analyser	Malvern Zetasizer, UK
9	FT IR Spectrophotometer	Bruker, Germany
10	Transmission electron microscope (TEM)	CM-200 Philips , India
11	FEG-SEM EDAX	JSM 7600F, JEOL, Japan
12	BET Analyzer	ASAP 2020 V4.01 Surface Area Analyzer, Micromeritics, US
13	X-Ray diffractometer	Nano-viewer, Rigaku, Japan
14	Incubator	JGUAN quality system, India

4.1. Synthesis of mesoporous silica nanoparticles:

Two different type of mesoporous silica nanoparticles have been synthesized: MCM-41 and SBA-16. The major difference in the synthesis of both type of nanoparticles is shown in table 4.3.

Table 4.3: Comparison of synthetic parameters of MCM-41 and SBA-16 type of MSNs.

Sr. No.	Parameters	MCM-41	SBA-16
1	pH condition	Alkaline	Acidic
2	Template/surfactant	CTAB	Poloxamer 407
3	pH regulator	Ethyl acetate or 1N HCl	Concentrated HCl

4.1.1 Synthesis of MCM-41 type of MSNs:

MCM-41 type of MSNs were synthesized using previously described procedure with little modification as described: [1]

In a typical procedure, a desired quantity of CTAB was mixed with 14 mL of isopropyl alcohol (IPA) and 200 mL of deionized water until complete dissolution in a polypropylene bottle. Suitable quantity of Na_2SiO_3 was dissolved in 33 mL of deionized water, separately. Then both solutions were cooled at 4 °C followed by slowly drop wise addition of Na_2SiO_3 solution to CTAB solution under vigorous stirring. Subsequently, the resulting mixture was sonicated for 1.5 h. Then 20 mL of pH regulator was added, and the solution was sonicated further for about 5 min. This solution was kept at 30 °C under magnetic stirring up to 5 h. Finally, the solution was kept at 80 °C for 72 h for aging. The resulting white solid was separated by filtration and washed several times with deionized water and methanol, dried at room temperature. The surfactant was removed by calcining at 540 °C for 6 h in air at heating rate of 1 °C/min.

Table 4.4 represents the various batches undertaken and the variables used in the synthesis of MCM-41 type of MSNs.

The best MSNs obtained were compared with the MCM-41 type of MSNs synthesized using TEOS as well as marketed MCM-41.

Table 4.4: Synthesis of MCM-41 type of MSNs.

Batch code	CTAB (gm)	Sodium Silicate (ml)	IPA (ml)	pH regulator	Aging temp. (°C)	Aging time (Hr)	Calcination temp. (°C)
F1	5	7	14	Ethyl acetate	80	72	540
F2	5	6	14	Ethyl acetate	80	72	540
F3	5	6	14	None	80	72	540
F4	5	6	14	HCl	80	72	540

4.1.2 Synthesis of SBA-16 type of MSNs:

SBA-16 type of MSNs were synthesized under acidic condition using sodium silicate as a silica precursor.

1 g of a structure directing agent, poloxamer 407, was dissolved in a mixture of 144 ml deionized water with 13.9 ml concentrated HCl with stirring for 30 minutes. Selected co-solvent was added in specified quantity and then required quantity of Na_2SiO_3 was added under stirring and the stirring was continued for another 24 h followed by aging at 100 °C temperature for 24 h in an oven. The resulting white solid was separated by filtration and washed several times with deionized water and methanol, dried at room temperature. The surfactant was removed by calcining at 540 °C for 6 h in air at heating rate of 1 °C/min.

Table 4.5 represents the various batches undertaken and the variables used in the synthesis of SBA-16 type of MSNs.

Table 4.5: Synthesis of SBA-16 type of MSNs.

Batch code	Poloxamer 407 (gm)	Sodium Silicate (ml)	Rate of addition	Co-solvent		Aging time (Hr)	Calcination temp. (°C)
				Type	Quantity (ml)		
SB1	1	5	Flush addition	IPA	2	24	540
SB2	1	3	Flush addition	IPA	3	24	540
SB3	1	2	Flush addition	IPA	5	24	540
SB4	1	5	Drop wise*	IPA	2	24	540
SB5	1	3	Drop wise*	IPA	3	24	540
SB6	1	2	Drop wise*	IPA	5	24	540
SB7	1	5	Drop wise**	IPA	2	24	540
SB8	1	3	Drop wise**	IPA	3	24	540

SB9	1	2	Drop wise**	IPA	3	24	540
SB10	1	3	Drop wise**	Butanol	3	24	540
SB11	1	2	Drop wise**	None	3	24	540

*** Dilution 1 in 10; ** Dilution 1 in 20**

4.2. Synthesis of metal oxide loaded mesoporous silica nanoparticles:

Various researchers have proved that metal oxide (MO) nanoparticles such as copper oxide (CuO)[2-5] nanoparticles and zinc oxide (ZnO)[6,7] nanoparticles can be used for diagnostic and anti tumor therapy.

MO-MSNs were synthesized according to literature procedures with some modifications:[8]

Required quantity of CTAB and polyethylene glycol 4000 (PEG 4000) were dissolved in 50 mL of deionized water. Separately, required amount of Na_2SiO_3 solution was mixed with 80 mL of deionized water and added drop wise to CTAB solution (rate of addition: 1ml/min) while the solution was stirred. This mixture was vigorously stirred for 1 h at 30°C. Ethyl acetate was added drop wise to adjust the pH value of the mixture to 9.0. After pH adjustment, the white mixture was stirred at 30°C for 1 h in a water bath. Suitable metal chloride (100mg in 10ml deionized water) was added drop wise and heated at 110°C for 24h and then cooled to room temperature. The resultant product was filtered, washed and dried at 80°C for 12 h to produce metal hydroxide loaded MSNs. The sample was calcined at a heating rate of 2°C/min to 550°C and maintained at this temperature for 5h to remove the template and produce MO-MCM-41.

Table 4.6: Synthesis of MO-MSNs.

Batch code	CTAB (gm)	Sodium Silicate (ml)	PEG 4000 (gm)	$CuCl_2$ (mg)	$ZnCl_2$ (mg)	Aging temp. (^oC)	Aging time (Hr)	Calcination temp. (^oC)
MO1	1	1.2	1	100	-	110	24	550
MO2	1	1.2	1	300	-	110	24	550
MO3	1	1.2	1	-	100	110	24	550
MO4	1	1.2	1	-	300	110	24	550

4.3. Characterization:

4.3.1. Physicochemical characterization:

The synthesized MSNs and MO-MSNs were characterized for various physicochemical parameters such as nature, colour and odour by visual inspection. Density of the nanoparticles was measured by using graduated measuring cylinder. The percent yield was also calculated as follow:

$$\% \, yield = \frac{\text{Weight of nanoparticles}}{\text{Weight of silica added}} * 100 \qquad (4.1)$$

4.3.2. Other characterization:

The standard characterization of mesoporous silica nanoparticles include use of dynamic light scattering (DLS) using which the hydrodynamic diameter of the particles can be measured. Nitrogen adsorption/desorption analysis [Brunauer Emmett Teller (BET) analysis and Barrett, Joyner, and Halenda (BJH)] is used to calculate the surface area, pore size, and pore volume. Electron microscopies such as scanning electron microscopy (SEM) can provide information regarding the surface morphology of nanoparticles, while

transmission electron microscopy (TEM) is used to detect the ordered arrangement of pores. Small angle X-ray diffraction (SAXD) is used to measure the periodic-ordered structure of the nanoparticles.[9-10]

Apart from these, UV-Visible spectrophometric technique was used to measure the copper content in CuO-MSN and Atomic Absorption spectroscopy (AAS) was utilized to detect metal content in MO-MSNs. Energy Dispersive X-Ray (EDX) Analysis was also performed to get the information about the elemental composition of the synthesized MSNs.

In the following section, the characterization techniques used have been discussed.

4.3.2.1 Particle size distribution (Dynamic light scattering):[11-13]

Dynamic light scattering (DLS) also known as photon correlation spectroscopy (PCS), is a very powerful, rapid non-invasive technique used to measure the size and size distribution and the polydispersity index (PI) of a sample. In DLS, interaction of sample with monochromatic wave of light helps to determine nanoparticle size, generally through detection of the signal by appropriate detector at an observation angle of 90̊. In DLS speed of particles undergoing Brownian motion is measured based on the fact that the smaller particles fluctuate more rapidly than the large ones. (Figure 4.1)

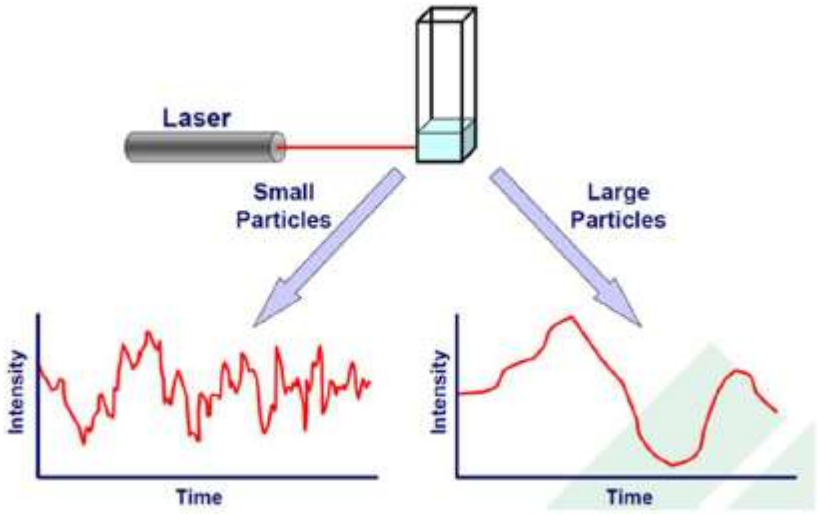

Figure 4.1: Fluctuation in intensity of light due to difference in particle size.[13]

Nano ZS zetasizer (Malvern Instruments, UK) was used to determine the particle size of nanoparticles. The nanoparticles were suspended in doubled distilled water at concentration less than 5mg/ml and sonicated prior to measurement of particle size. The measurements were carried out in an automatic mode and the values were presented as an average value of 20 runs.

- **Zeta Potential:**[13,14]

The electrokinetic or zeta-potential is an important parameter of the electrical double layer and represents a characteristic of electrical properties of solid/liquid and liquid/gaseous interfaces. In contact with a polar medium (water), the majority of particles show a definite surface charge as the consequence of ionization, ionic adsorption and ionic dissolution. This surface charge influences the arrangement of neighbouring ions. Thus, it is related to the net electrostatic repulsion between the particles. Furthermore, it is also an important parameter to predict the biological interactions with blood protein, cell surface phagocytes and other molecules.

To measure the zeta potential, the nanoparticles were suspended in doubled distilled water at concentration less than 5mg/ml and sonicated prior to measurement. The measurements were carried out in an automatic mode and the values were presented as an average value of 20 runs.

4.3.2.2 Morphological characterization:

Morphological characterization of the synthesized MSNs was performed using two different electron microscopy techniques:

(1) Scanning electron microscopy (SEM), and

(2) Transmission electron microscopy (TEM)

Electron microscopes uses a beam of electrons to generate an image. The basic principles for electron microscopes is same as that of the light microscope but here electrons are used instead of light which make these microscopes capable of much higher magnifications and provide a greater resolving power than a light microscope, allowing it to see much smaller objects in finer detail.

- **Scanning electron microscopy (SEM):[15]**

Although first developed in the early 1930's and perfected to a high degree in the late 1950's, the scanning electron microscope have been slow to find their proper fields of application. In 1965 the scanning electron microscope became commercially available, and since then there has been a great spurt in use of this equipment as a research tool.

SEM is a characterization technique that is used widely for all types of samples, from hard materials such as metals and ceramics to soft materials such as polymers and biological tissues. Morphology of the synthesized nanoparticles was characterized using Field Emission Gun-Scanning Electron microscope (JSM 7600F, JEOL, Japan) operated at a voltage of 0.1 to 30.0 kv.

- **Transmission electron microscopy (TEM):[16-18]**

Max Knoll and Ernst Ruska of the Berlin Technische Hochschule demonstrated the first TEM in 1931, and in 1933 achieved a resolution greater than that of light with this microscope. Working at Siemens, Ruska helped to develop the first commercial TEM in 1939.

TEM is used to reveal sub-micrometer, internal fine structure (the microstructure or ultrastructure). TEM images of the nanoparticles were obtained on a CM-200 transmission electron microscope (Philips) operating at 20-200kv voltage with resolution of 2.4 Ao. The samples for TEM measurements were made by casting one drop of the samples on copper grids coated with carbon.

4.3.2.3 Nitrogen sorption analysis:[19,20]

The surface area is one of the most important quantities for characterizing novel porous materials. The BET analysis is the standard method for determining surface areas from nitrogen adsorption isotherms. It was originally derived for multilayer gas adsorption onto flat surfaces. The BET analysis assumes that adsorption occurs by multilayer formation and that the number of adsorbed layers is infinite at the saturation pressure, i.e., adsorption occurs as if on a free surface.

The surface area was evaluated with nitrogen adsorption-desorption isotherm measurements on a ASAP 2020 V4.01 Surface Area Analyzer (Micromeritics Corp., USA) at −195.8 °C. The nanoparticles were degassed at 50 °C overnight before analysis. The surface areas were calculated with BET theory using isotherm adsorption data at P/P_0 from 0.01 to 0.99.

$$SA_{BET} = \frac{CSA \times N_A}{22414 \times 10^{18} \times (S + Y_{INT})} \quad (4.2)$$

Where, SA_{BET} is the BET surface area (m^2/g);

CSA is the analysis gas molecular cross-sectional area (0.162 nm^2 for N_2);

Na is the Avogadro constant 6.023×10^{23};

S is the slope (g/cm^3);

YINT is the Y-intercept (g/cm^3).

- **BJH method:**

The pore volume and pore size distributions were obtained from an adsorption branch by using the Barrett, Joyner and Halenda (BJH) method.

$$r_p = \frac{4.15}{\log(\frac{P_0}{P})} + 3.54 \times \left(\frac{-5}{\ln(\frac{P}{P_0})}\right)^{0.333} \quad (4.3)$$

Where r_p is pore radius (Å).

4.3.2.4 X-Ray diffraction (XRD) analysis:[21]

XRD is a potent nondestructive method which provides information on structures, phases, preferred crystal orientations (texture), and other structural parameters, such as average grain size, crystallinity, strain, and crystal defects in the material. XRD peaks are produced by constructive interference of a monochromatic beam of X-rays scattered at specific angles from each set of lattice planes in a sample. The peak intensities are determined by the distribution of atoms within the lattice. Consequently, the XRD pattern is the fingerprint of periodic atomic arrangements in a given material.

XRD patterns of MSNs were obtained on Nano-viewer (Rigaku, Japan), to confirm the crystalline structure of the particles and find out periodic atomic arrangements within the sample. The instrument utilized Cu-Ka X-rays operated at 45 kV and 60 mA.

4.3.2.5 Elemental Analysis:[22,23]

Energy dispersive X-ray spectrometry (EDX/EDS) is a widely applied elemental microanalysis method capable of identifying and quantifying all elements in the periodic table except H, He, and Li. EDS is a spectroscopic technique that determines the presence and relative abundance of the elements that compose the surface of the specimen under study. The X-ray photons that are produced when an energetic electron beam reaches the surface are detected and their energy depends on which atom they came from.

SEM coupled with EDS are two analysis techniques that are widely used to study all kinds of solid samples, from inorganic to biological. They are used to determine morphological features of interest at a micron and sub-micron level as well as to study the chemical composition of the samples in terms of the amount of each element present.

Morphology of the synthesized nanoparticles along with their chemical composition was characterized using FEG-SEM-EDS (JSM 7600F, JEOL, Japan) operated at a voltage of 0.1 to 30.0 kv.

4.3.2.6 Atomic absorption spectroscopy (AAS):[24-27]

The atomic absorption method of analysis as first described by Walsh et al. has been found to be extremely suitable for the rapid determination of various elements such as magnesium, zinc, iron, manganese, and copper.

Atomic absorption spectroscopy is based on the measurement of the amount of light at the resonant wavelength which is absorbed as the light passes through a cloud of atoms. The amount of light absorbed increases with increase in the number of atoms in the light path. By measuring the amount of light absorbed, a quantitative determination of the amount of analyte element present can be made. The use of special light sources and careful selection of wavelength allow the specific quantitative determination of individual elements in the presence of others.

Accurately weighed amount (10 mg) of MO-MSNs (M= Cu or Zn) was reacted with the required amount of concentrated HCl to produce MCl_2 salt and diluted upto 10 ml using deionised water to produce stock solution (1000 µg/ml). It was further diluted by transferring 0.2 ml of stock solution to 10 ml volumetric flask and volume was made up to 10 ml using deionised water to make 20 µg/ml. The amount of metal in respective solutions was measured by using Atomic Absorption Spectrometer AAnalyst 200 (Perkin Elmer) (At Chemistry Department, Faculty of Science, The Maharaja Sayajirao University of Baroda).

4.3.2 Chick chorioallantoic membrane (CAM) assay:

Various researchers have shown anti angiogenic effect of CuO nanoparticles as well as ZnO nanoparticles.[28,29] CAM assays have been widely used to study angiogenesis[30], tumor cell invasion and metastasis[31-33]. The CAM model possess many advantages, such as

(a) The highly vascularized nature of the CAM greatly promotes the efficiency of tumor cell grafting;

(b) High reproducibility;

(c) Simplicity and cost effectiveness, and finally

(d) As the CAM assay is a closed system, it allows experimental study of potential anti-metastatic compounds that are only available in small quantities.[34]

Fifteen fertilized white chicken eggs were obtained from Goverment poultry house, Vadodara, India. They were carefully cleaned with 70% alcohol and divided into five groups (three eggs in each group); group 1 was control (without any treatment); and four other groups were experimental (groups 2 and 3 were treated with formulation containing copper (batch MO1 and MO2) while groups 4 and 5 were treated with formulation containing zinc (batch MO3 and MO4) at concentrations of 20 µg/ml of NPs. Eggs were incubated in an incubator at 37 °C with 60% humidity for 2 days. A small window was made in the shell of each egg on day 3 under aseptic conditions. The window was resealed with adhesive tape and eggs were returned to the incubator until day 10 of chick embryo development. On the 11th day of incubation, each specified group was treated with MO-MSNs under aseptic condition. Then, the windows were resealed and the incubation was

continued for further 72 h. At the day 14 of incubation, the egg shells were softly removed and CAM were examined for development or inhibition of veins.[29,35]

4.4 Results and discussion:

4.4.1 Physicochemical Characterizations:

Various physicochemical parameters of the synthesized MCM-41 type of MSNs, synthesized under alkaline conditions, are shown in Table 4.7. No significant impact of variables was observed on any physicochemical parameters (except yield) of the synthesized MSNs. All the MCM-41 type of MSNs were white coloured, odourless smooth powder (except batch F4 which formed coarse rough powder) with density near 0.31 ± 0.03 g/ml. The yield of each synthesis was found higher than 90% except batch F3 in which the yield obtained was just 14.3 %. This low yield might be due to very less degree of polycondensation of the silicate species at highly alkaline reaction conditions. Hence, it can be said that the addition of the pH regulator facilitated the polycondensation of the silicate species and improved the yield to great extent. No difference in the physicochemical parameters of MSNs, synthesized using different concentration of sodium silicate was observed but the change in the pH regulator such as ethyl acetate or HCl remarkable affected the synthesis of MSNs. Coarse aggregated white powder was observed in case of HCl which might be due the difference in the acidity of HCl and ethyl acetate. HCl is a strong acid and it reduces the pH of the reaction mixture faster as compared to ethyl acetate. As compared to monomeric alkoxide silica precursors such as TEOS or TMOS, sodium silicate undergo very quick polymerization with decrease in the pH. So, the rate of polymerization of silicate species must be higher upon addition of HCl as compared to ethyl acetate. This might have lead to formation of coarse particles. Furthermore, ethyl acetate is known to affect the pore structure formation as it act as a good co-solvent for CTAB.

Based on these observations, further analysis was performed using the batches in which fine powdered MSNs were formed (F1 and F2) and the batches with less yield and coarse aggregates were eliminated.

Table 4.7: Physicochemical Characterizations of MCM-41 type of MSNs.

Batch No.	**F1**	**F2**	**F3**	**F4**
Nature	Solid fine powder	Solid fine powder	Solid fine powder	Solid coarse powder
Colour	White	White	White	White
Odour	None	None	None	None
Yield (%)	91.2	92.8	14.6	91.7
Density (g/ml)	0.28	0.31	0.29	0.34

Table 4.8 represent the physicochemical parameters of SBA-16 type of MSNs synthesized under acidic condition. As seen in the table, the yield of each batch was found greater than 90%. Though, all the synthesized MSNs were white in colour, odourless with density around 0.32 ± 0.05 g/ml, a significant difference in the physical appearance of MSNs was observed. In case of batches SB1-SB6, large precipitates of silica were observed immediately upon addition of sodium silicate solution to the reaction mixture and they led to the formation of very hard aggregates of silica particles. Drop wise addition of silicate solution showed little decrease in the size of aggregates but addition and changing the concentration of co-solvent didn't make any significant difference. This might be due to the fact that sodium silicate species undergo very quick polymerization with decrease in pH. Hence, to reduce the rate of polymerization, Na_2SiO_3 solution was further diluted to much more extent and added drop wise very slowly. This lead to formation of fine powdered MSNs. Thus, the rate of addition and concentration of silica precursor at the time of addition were found critical parameters for the synthesis of MSNs under acidic condition when sodium silicate is used as a source of silica. When these parameters were controlled, change in the concentration of co-solvent or type of co-solvent didn't make any

significant difference in the synthesized MSNs. White coarse particles were formed in case of batch SB-7 which might be due to very high concentration of sodium silicate.

Based on these observations, batches SB1-SB7 were eliminated from further analysis.

Table 4.8: Physicochemical Characterizations of SBA-16 type of MSNs.

Batch No.	**Nature**	**Colour**	**Odour**	**Yield (%)**	**Density (g/ml)**
SB1	Solid Clumps	White	None	94.2	0.33
SB2	Solid Clumps	White	None	93.7	0.34
SB3	Solid Clumps	White	None	93.8	0.34
SB4	Solid Clumps	White	None	92.6	0.32
SB5	Solid Clumps	White	None	93.1	0.35
SB6	Solid Clumps	White	None	94.1	0.32
SB7	Solid coarse powder	White	None	92.4	0.28
SB8	Solid	White	None	91.9	0.29
SB9	Solid	White	None	91.5	0.27

SB10	Solid	White	None	91.1	0.28
SB11	Solid	White	None	91.3	0.31

Metal oxide loaded MSNs were synthesized under basic conditions due to the fact that sodium silicate forms NaOH in the reaction mixture and this NaOH can oxidize the metal halide leading to the formation of metal hydroxide. Upon calcination these metal hydroxides gets converted to the metal oxide. The physicochemical properties of different synthesized MO-MSNs are shown in table 4.9. The grayish colour of the CuO loaded MSNs might be due to black coloured CuO incorporated with the MSNs framework. ZnO loaded nanoparticles were white in colour. All the MO-MSNs were found odourless, smooth powder with density near 0.25 ± 0.01 g/ml and produced the yield more than 90%.

Table 4.9: Physicochemical Characterizations of MO-MSNs.

Batch No.	**MO1**	**MO2**	**MO3**	**MO4**
Nature	Solid fine powder	Solid fine powder	Solid fine powder	Solid fine powder
Colour	Grayish	Grayish	White	White
Odour	None	None	None	None
Yield (%)	91.5	90.6	90.9	90.4
Density (g/ml)	0.25	0.26	0.25	0.25

4.4.2 Particle size distribution and zeta potential:

The hydrodynamic diameter and size distribution of MCM-41 and SBA-16 type of MSNs as well as MO-MSNs was measured using Nano ZS zetasizer and shown in Table 4.10.

Table 4.10: Particle size analysis and zeta potential of synthesized MSNs.

Batch No.	**F1**	**F2**	**SB8**	**SB9**	**SB10**	**SB11**	**MO1**	**MO2**	**MO3**	**MO4**
Particle size (nm)	685.5	113	668.8	566.3	754.6	580.7	140.0	443.6	257.2	490.4
Zeta Potential (mV)	-41.3	-35.6	-33.7	-32.1	-32.6	-34.2	-27.7	-21.6	-30.2	-26.4

As seen in figure 4.2, in case of MCM-41 type of MSNs, batch F2 was found to have size below 200 and lesser than batch F1. Both the batches showed negative charge which might be due to surface silanol groups. The higher size detected in case of batch F1 might be due to higher concentration of silicates which are also responsive for higher negative charge due to more surface silanol groups.

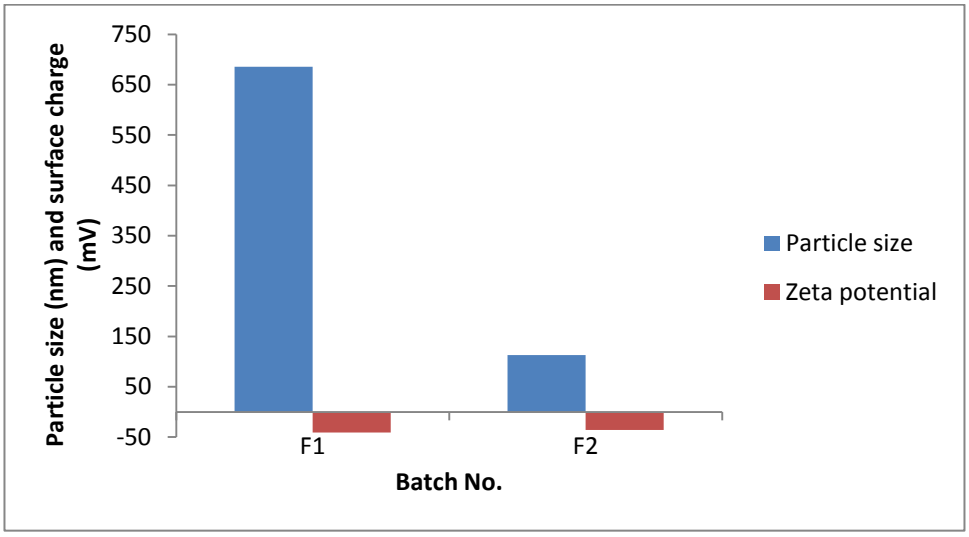

Figure 4.2: Particle size and zeta potential of MCM-41 type of MSNs.

Figure 4.3 represents the change in particles size of different SBA-16 type of MSNs while figure 4.4 shows zeta potential of different SBA-16 type MSNs. All the particles were found to have size over 500 nm and highly negative zeta potential. As compared to butanol, IPA was found to be good co-solvent as the particle size obtained in case of IPA was lesser than that of butanol. Futher more the particle size was found to reduce with decrease in the sodium silicate concentration. The negative zeta potential might be due to high density of silanol groups while larger size might be because of uncontrolled polycondensation of silicate species under acidic environment.

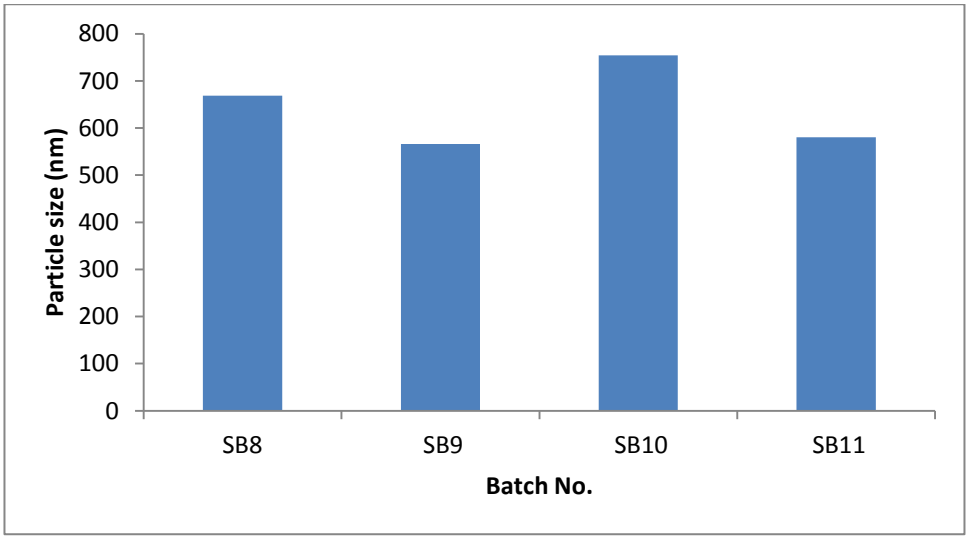

Figure 4.3: Particle size of different SBA-16 type of MSNs.

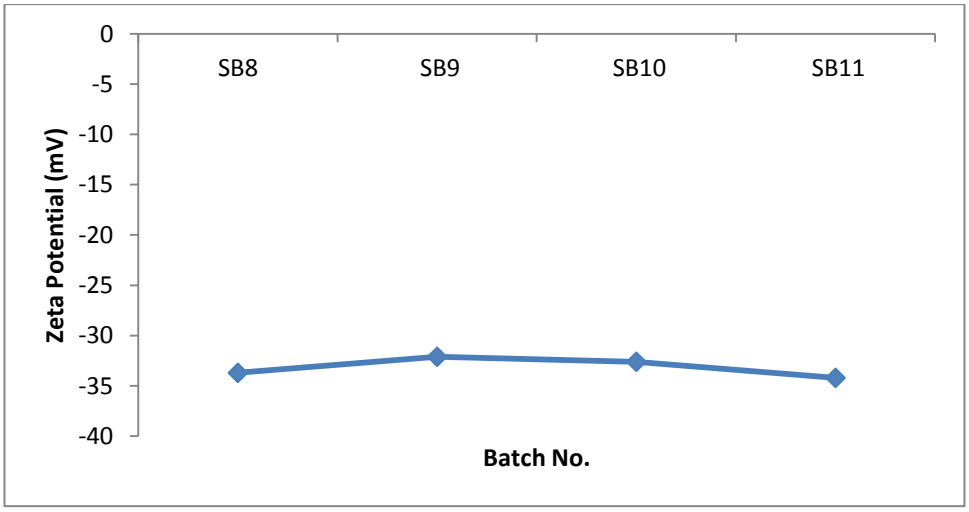

Figure 4.4: Zeta potential of different SBA-16 type of MSNs.

Figure 4.5 and 4.6 represent the graphical demonstration of particle size and zeta potential of different batches of MO-MSNs respectively. As seen in figure 4.5, MO1 and MO3 were having particle size lesser than MO2 and MO4. Less amount of metal chloride was added initially during the synthesis of both MO1 and MO3 and hence it can be said that the addition of metal chloride during synthesis process might have some impact on the particle size. Further, the zeta potential of all MO-MSNs was negative but it was lesser than the zeta potential of MCM-41 type of MSNs. This decrease in negative zeta potential might be due to incorporation of MO within MSN framework which can interact with the silanol groups present over inner surface of pore wall and thereby decrease the amount of free silanol groups. This can lead to reduction in the zeta potential.

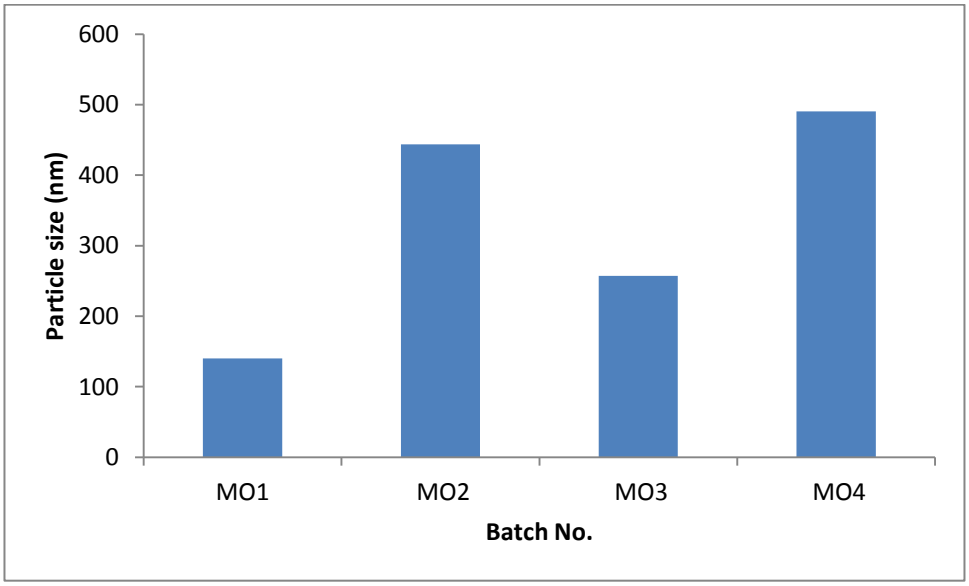

Figure 4.5: Particle size of different MO-MSNs.

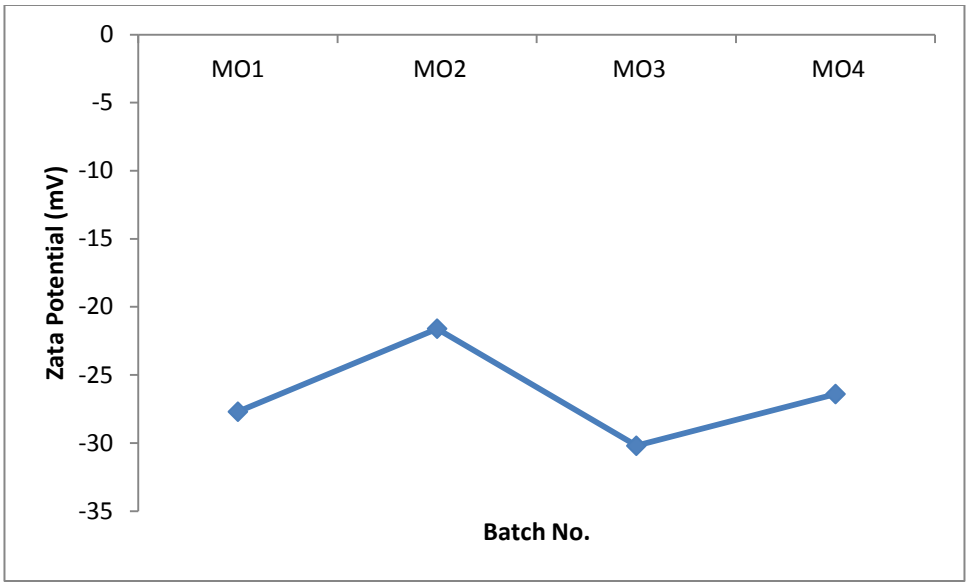

Figure 4.6: Zeta potential of different MO-MSNs.

4.4.3 Determination of metal content in MO-MSNs:

The copper content in the CuO-MSNs (Batch MO1 and MO2) while the zinc content in ZnO-MSNs (Batch MO3 and MO4) was determined using atomic absorption spectroscopy. The results showed that the loading of copper loaded into the MSNs was much higher as compared to the Zn. This might be due to high solubility of intermediate $Zn(OH)_2$ in sodium hydroxide to form zincate ions and then subsequent removal of them while washing. Batch MO2 was found to contain higher copper (about 6.447% Cu) as compared to batch MO1 (about 2.91% Cu). This was due to lesser copper content addition in batch MO1 during synthesis procedure. Similarly batch MO4 was found to contain higher zinc (about 0.238% of Zn) content as compared to batch MO3 (about 0.06% of Zn).

Table 4.11: Determination of metal content in different MO-MSNs by AAS.

Batch No.	**MO1**	**MO2**	**MO3**	**MO4**
Copper content (%)	2.91	6.45	-	-
Zinc content (%)	-	-	0.06	0.24

4.4.4 Anti-angiogenic activity (CAM assay):

CAM assay was performed to check the anti-angiogenic activity of MO-MSNs and to confirm whether the metal oxide loaded MSNs can inhibit the angiogenesis or not. As shown in Figure 4.7, the angiogenesis indicators (number and length of the newly formed arterioles) were not significantly decreased in control and groups treated with ZnO-MSNs (batch MO3 and MO4). While in case of CuO-MSNs, a significant reduction in number of newly formed arterioles as well as breaking down of blood vessels in CAM was observed. MO2 formulation was found to inhibit angiogenesis completely. This showed that CuO possessed higher anti-angiogenic activity.

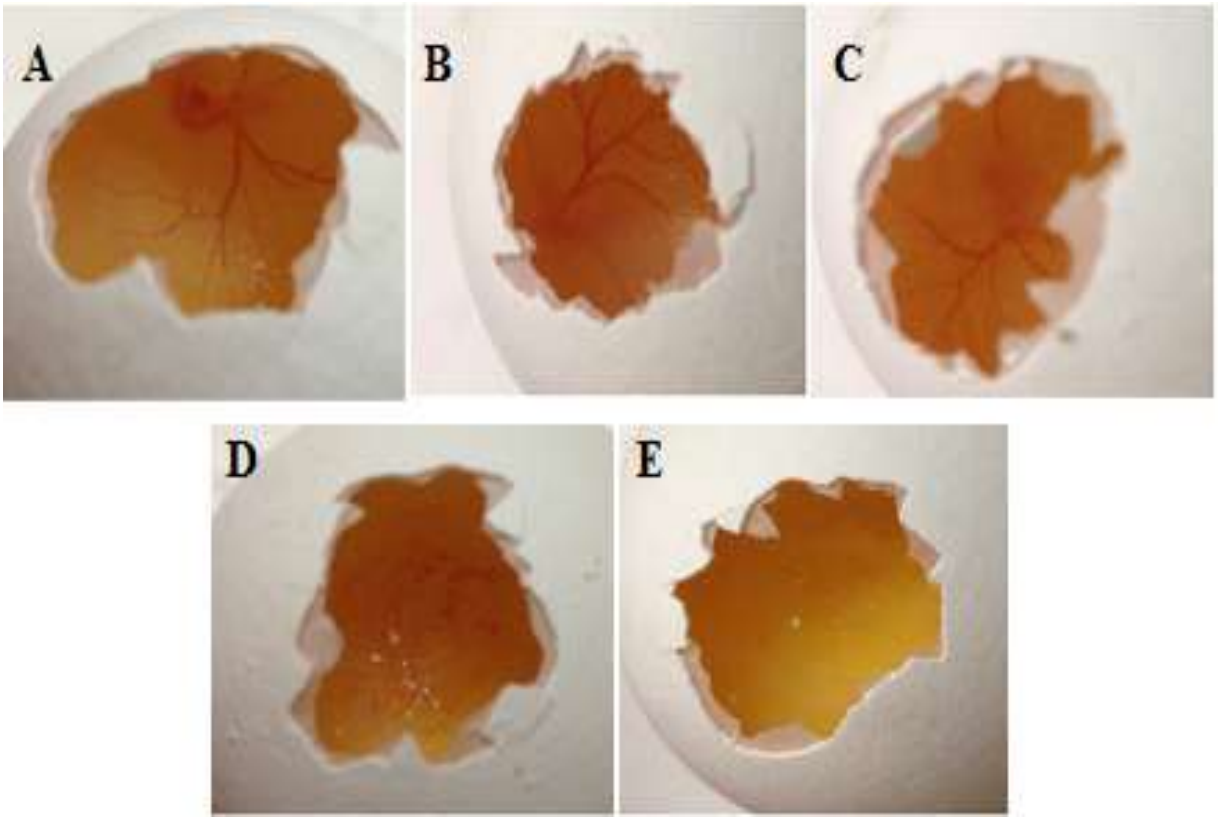

Figure 4.7: Anti-angiogenic activity of MO-MSNs studied by performing CAM assay: Control (A), Treatment groups (Batch MO3=B, MO4=C, MO1=D and MO2=E).

4.4.5 Nitrogen adsorption/desorption study:

The specific surface areas were obtained by the Brunauer–Emmett–Teller (BET) method and pore size diameters were achieved from the desorption branches of the isotherms by BJH methods. The BET surface area, average pore size diameter and pore volume of MSNs synthesized under alkaline conditions and MSNs synthesized under acidic conditions as well as MO-MSNs are represented in Table 4.12.

Table 4.12: The BET surface area, pore size and pore volume of different MSNs.

Batch No.	BET surface area (m^2/g)	Pore size (nm)	Pore volume ($cm^3\ g^{-1}$)
F1	318.53	3.7	0.662
F2	849.13	2.5	1.073
SB8	140.11	29.78	0.1
SB9	181.81	22.18	0.1
SB10	55.33	34.08	0.09
SB11	14.53	44.21	0.03
MO1	568.30	2.7	0.742
MO2	532.27	2.4	0.624
MO3	345.21	4.2	0.496
MO4	329.86	3.9	0.467

From the table 4.12, it is clear that the MSNs synthesized under alkaline conditions (MCM-41 type) were having higher surface area and greater pore volume as compared to MSNs synthesized under acidic conditions (SBA-16 type). Under alkaline conditions, silicate

species are composed of small negatively charged oligomers which facilitate the formation of silica-surfactant assemblies while under neutral or acidic conditions they polymerize fast and make the formation of MSNs difficult. MO-MSNs represent surface area and pore volume in between MCM-41 type of MSNs and SBA-16 type of MSNs. The decrease in the surface area and pore volume of MO-MSNs as compared to MCM-41 type of MSNs might be due to incorporation of MO within MSNs framework which blocks the pores and there by reduces the surface area.

Figure 4.8 represent the surface area and pore volume of batch F2 and MO1. As seen in figure 4.8, N_2 adsorption and desorption isotherms for all the nanoparticles was found to exhibit a type IV isotherm corresponding to a cylindrical mesoscale pore structure. The sharp increase at a relative pressure of 0.2-0.8 (P/P_0) could be related to the capillary condensation of N_2 and narrow pore size distribution or uniform pore sizes.

SBA-16 type of MSNs were excluded from further studies because of their higher size and low surface area and pore volume. Based on the results obtained from particle size analysis, AAS study, CAM assay, Nitrogen adsorption/desorption analysis and in vitro cytotoxicity studies performed for plain MSNs and MO-MSNs (described in detail in chapter 7), Batch F2 was selected among MSNs and Batch MO1 containing CuO-MSN was selected among MO-MSNs for further studies. CuO-MSNs were preferred over ZnO-MSNs as they possessed smaller particle size and higher metal content due to which they showed superior anti-angiogenic activity in CAM assay and better cytotoxicity against MCF-7 breast cancer cell line. Furthermore, they were also found to have higher surface area and pore volume.

A

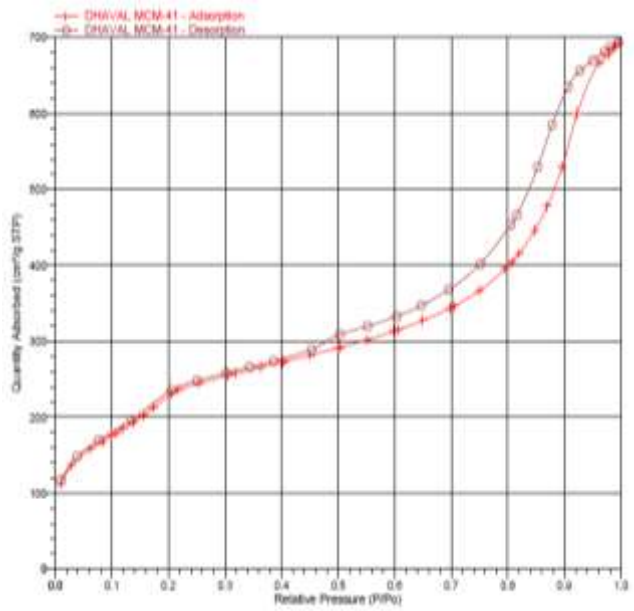
DHAVAL MCM-41 - Adsorption
DHAVAL MCM-41 - Desorption
Quantity Adsorbed (cm³/g STP)
Relative Pressure (P/Po)

B

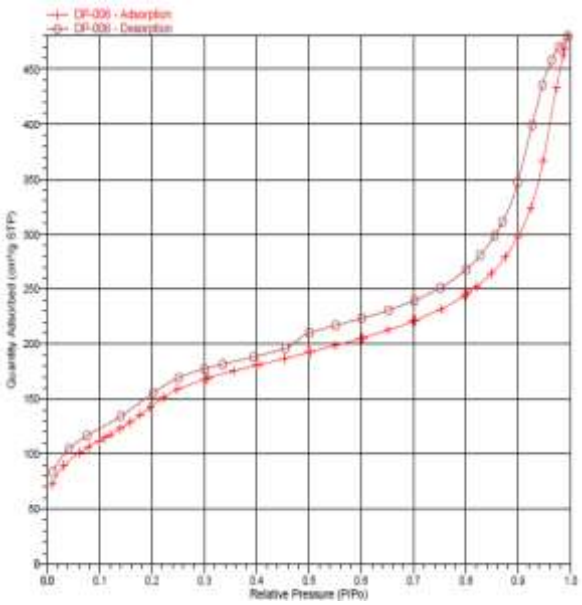
DF-006 - Adsorption
DF-006 - Desorption
Quantity Adsorbed (cm³/g STP)
Relative Pressure (P/Po)

C

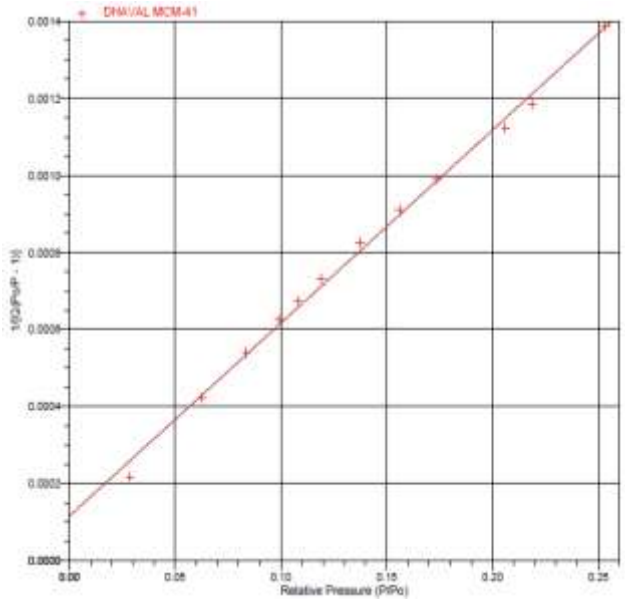
DHAVAL MCM-41
1/[Q(Po/P - 1)]
Relative Pressure (P/Po)

D

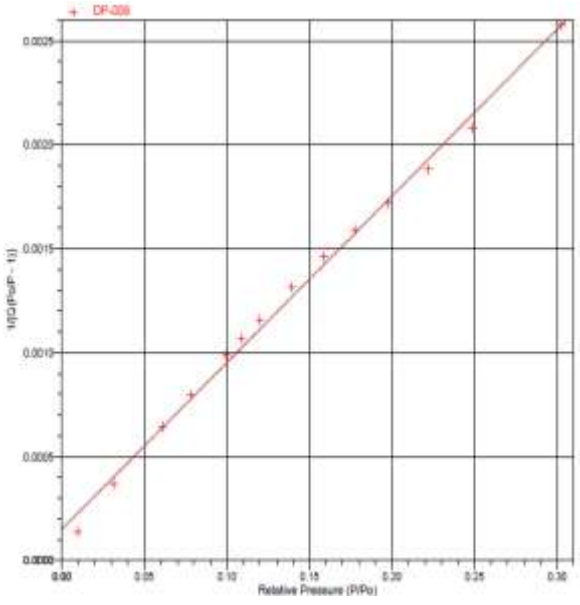
DF-006
1/[Q(Po/P - 1)]
Relative Pressure (P/Po)

E **F**

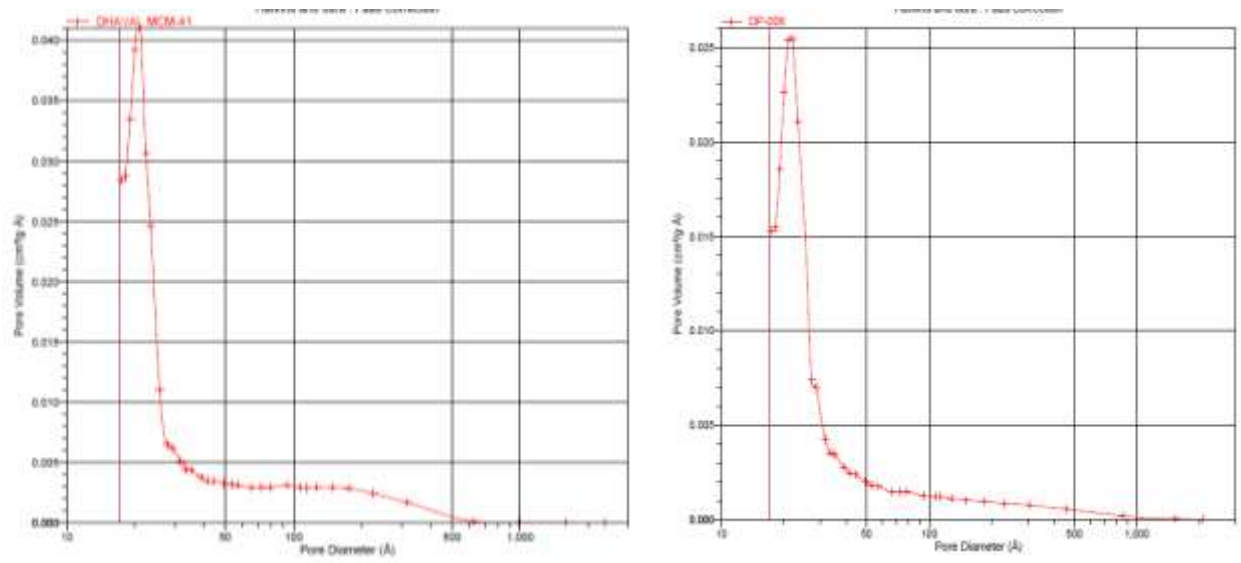

Figure 4.8: Graphical representation of the surface area and pore volume of MSNs (Batch F2) and CuO-MSNs (Batch MO1): Isotherm Linear Plot of MSNs, BET surface area plot and dV/dD Pore Volume of MSNs (A, C & E); Isotherm Linear Plot of MSNs, BET surface area plot and dV/dD Pore Volume of CuO-MSNs (B, D & F).

4.4.6 Morphological Characterizations:

Morphological Characterization of synthesized nanoparticles was performed using two different techniques: TEM and FEG-SEM.

- **TEM imaging:**

TEM images were captured with a view to analyze the physical morphology as well as pore channel structure of the synthesized MSNs and CuO-MSNs. As shown in Figure 4.9, both MSNs and CuO-MSNs were nearly spherical to elliptical in shape.A highly ordered mesoporous network with a hexagonal array and classified pores could be clearly seen in the pure MSN nanoparticles. Figure 4.9 (B) relates CuO-MSNs in which very small dark spots can be seen within particles representing the CuO loaded into the MSNs. The corresponding selected area electron diffraction (SAED) pattern is also shown with TEM

images and it clearly demonstrated amorphous structure of both MSNs and CuO-MSN nanoparticles.

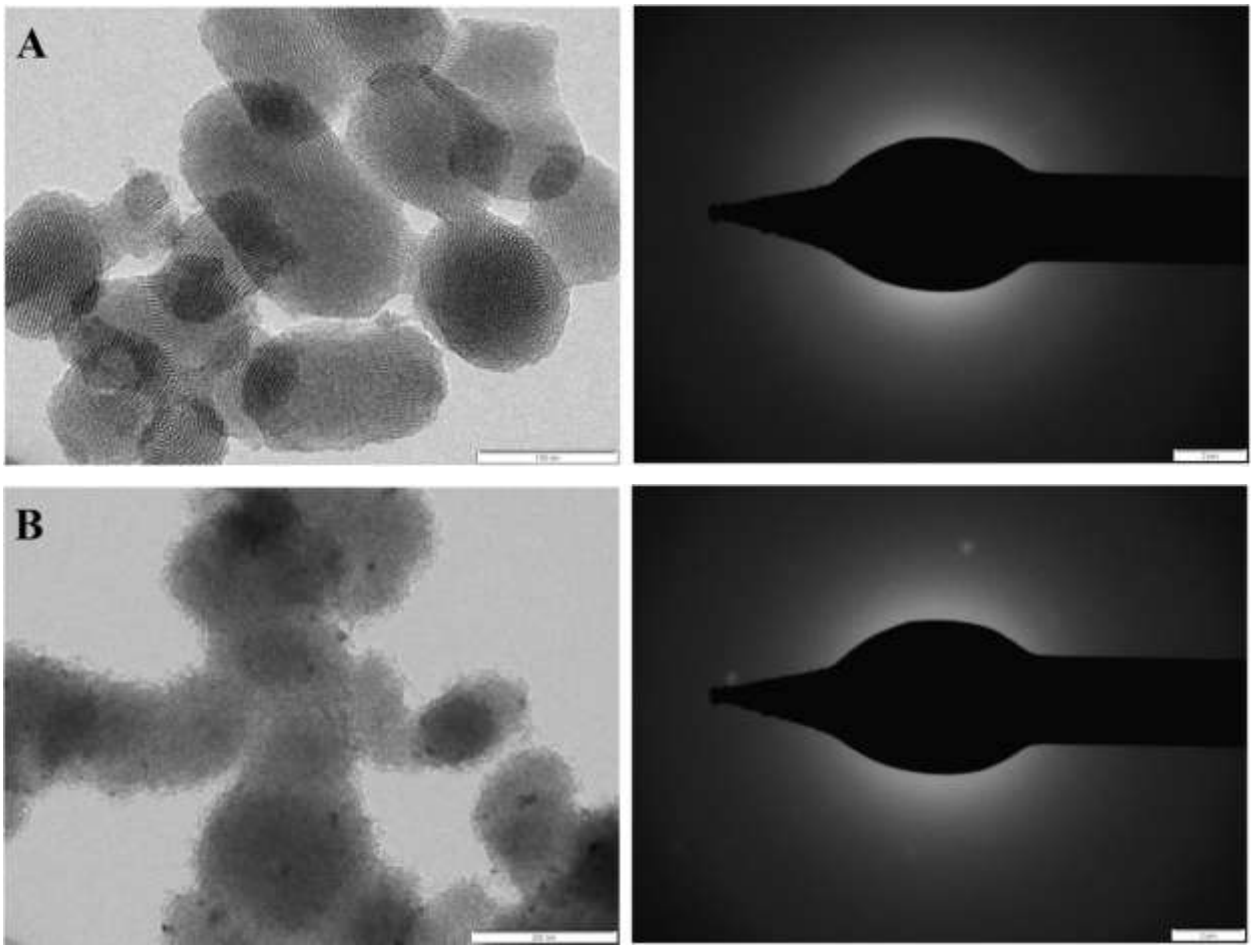

Figure 4.9: Morphological characterization of nanoparticles: TEM images with corresponding SAED for MSNs (A) and for CuO-MSNs (B).

- **FEG-SEM imaging:**

  The morphology of MSNs and Cuo-MSNs was further confirmed by FEG-SEM imaging. As seen in Figure 4.10, the nanoparticles were nearly spherical to elliptical in shape.

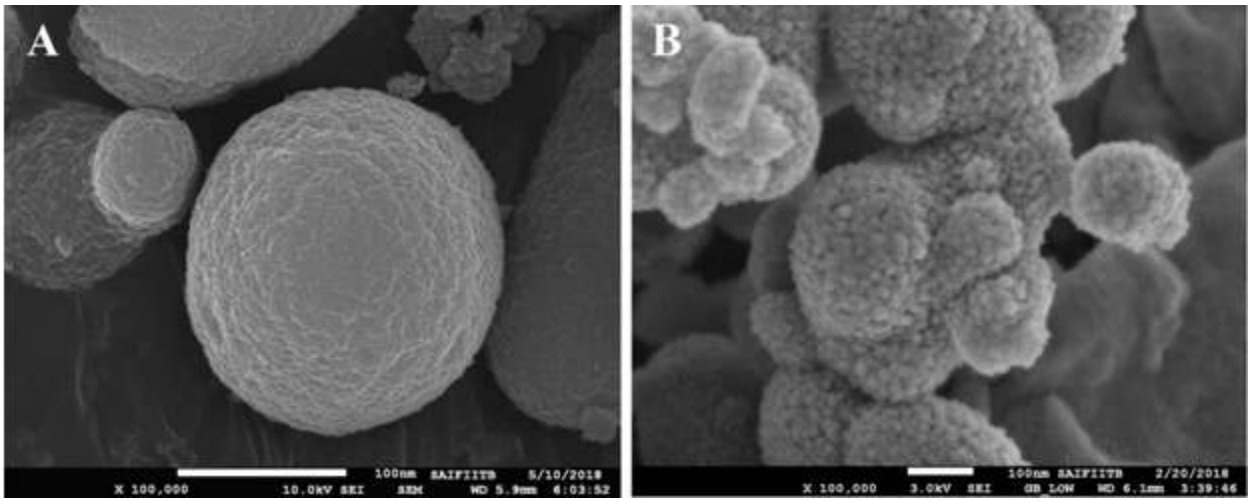

Figure 4.10: Morphological characterization of nanoparticles: FEG-SEM images of MSNs (A), and CuO-MSNs (B).

4.4.7 FEG-SEM-EDS mapping:

As, the mesoporous silica nanoparticles are synthesized using very economic silica source, sodium silicate, there is a probability that the synthesized nanoparticles might have incorporated high level of sodium within their structure. Furthermore, CuO-MSNs have also been synthesized which contain copper incorporated within their structure. Hence, these nanoparticles might have elemental composition different from MSNs synthesized using other silica source such as alkoxides (Tetra ethyl ortho silicate; TEOS). So, FEG-SEM-EDS mapping of the synthesized nanoparticles was performed with a view to confirm their elemental composition.

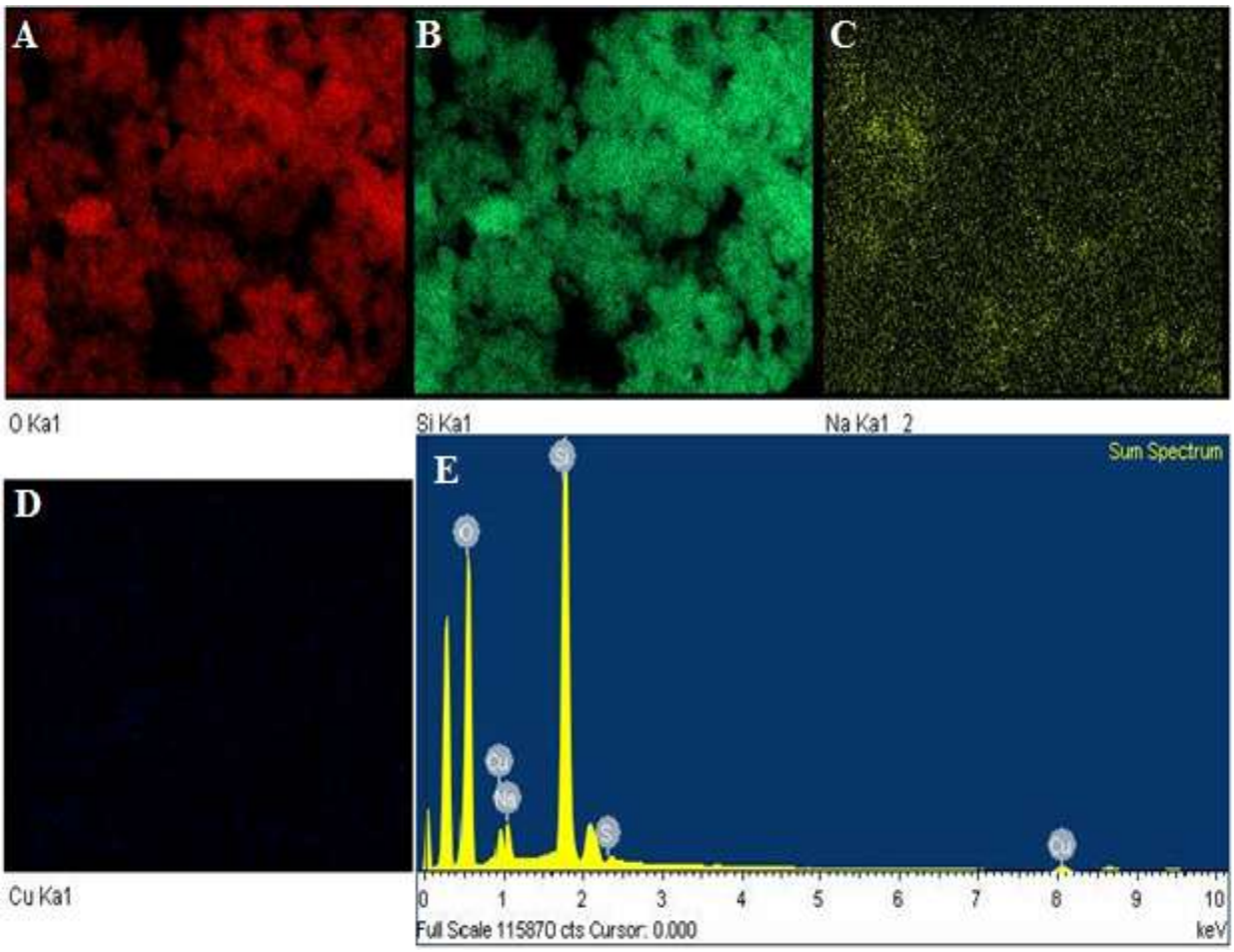

Figure 4.11: FEG-SEM-EDS mapping representing elemental composition of MSNs: Oxygen (A); Silicon (B); Sodium (C); Copper (D) and EDS spectrum (E).

Figure 4.11 represent the elemental composition of MCM-41 type of MSNs synthesized using commercial sodium silicate as a silica precursor and it clearly showed the presence of elemental sodium within the MSNs framework.

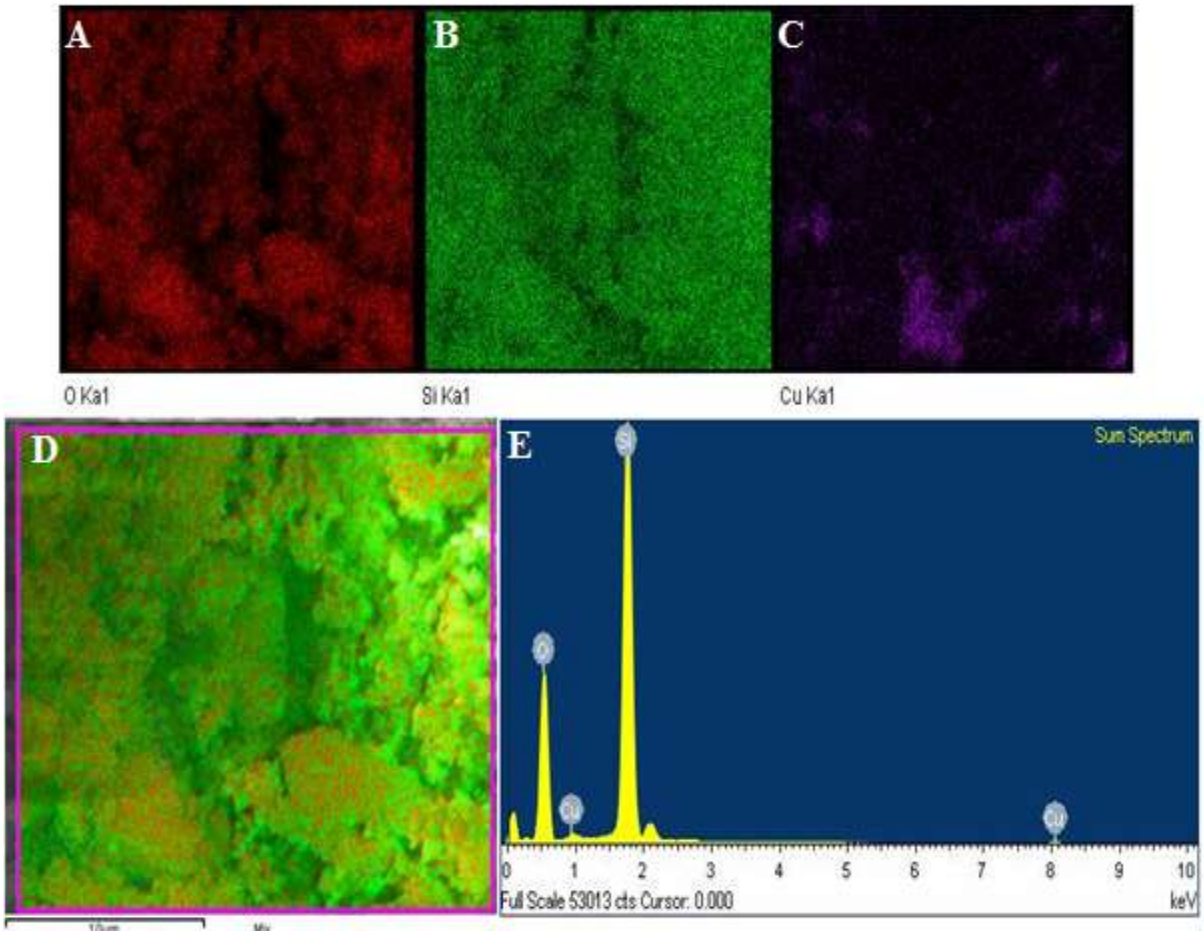

Figure 4.12: FEG-SEM-EDS mapping representing elemental composition of CuO-MSNs: Oxygen (A); Silicon (B); Copper (C); overlay (D) and EDS spectrum (E).

Figure 4.12 represent the elemental composition of CuO-MSNs. As compared to MSNs, the amount of Cu was found about 6.07 times higher in CuO-MSNs which clearly proved the incorporation of CuO within MSNs framework. Furthermore, uniform distribution of copper can be seen within selected area. This CuO incorporated within MSNs may impart synergistic cytotoxic effect in anticancer therapy.

Table 4.13: FEG-SEM-EDS: elemental composition of MSNs and CuO-MSNs.

Element	MSNs		CuO-MSNs	
	Weight %	**Atomic %**	**Weight %**	**Atomic %**
O	52.62	68.66	52.46	66.83
Si	42.77	31.84	44.26	32.12
Na	2.77	2.52	-	-
Cu	0.54	0.18	3.28	1.05

4.4.8 XRD analysis:

The amorphous structure of MSNs and CuO-MSNs was confirmed by XRD. Figure 4.13 (A) and 4.14 (A) represents small angle X-ray scattering (SAXS) pattern of MSNs and CuO-MSNs, respectively, in which four well-resolved diffraction peaks, assigned as (100), (110), (200), and (210) planes, respectively, are clearly observed, which is consistent with the characteristic diffraction pattern of MCM-41 type MSN. Figure 4.13 (B) represent wide angle X-ray scattering (WAXS) image of synthesized mesoporous silica nanoparticles in which absence of characteristic sharp diffraction peak confirmed the amorphous nature of synthesized material. Similarly Figure 4.14 (B) shows XRD image of CuO-MSNs in which characteristic peaks for CuO can be seen.

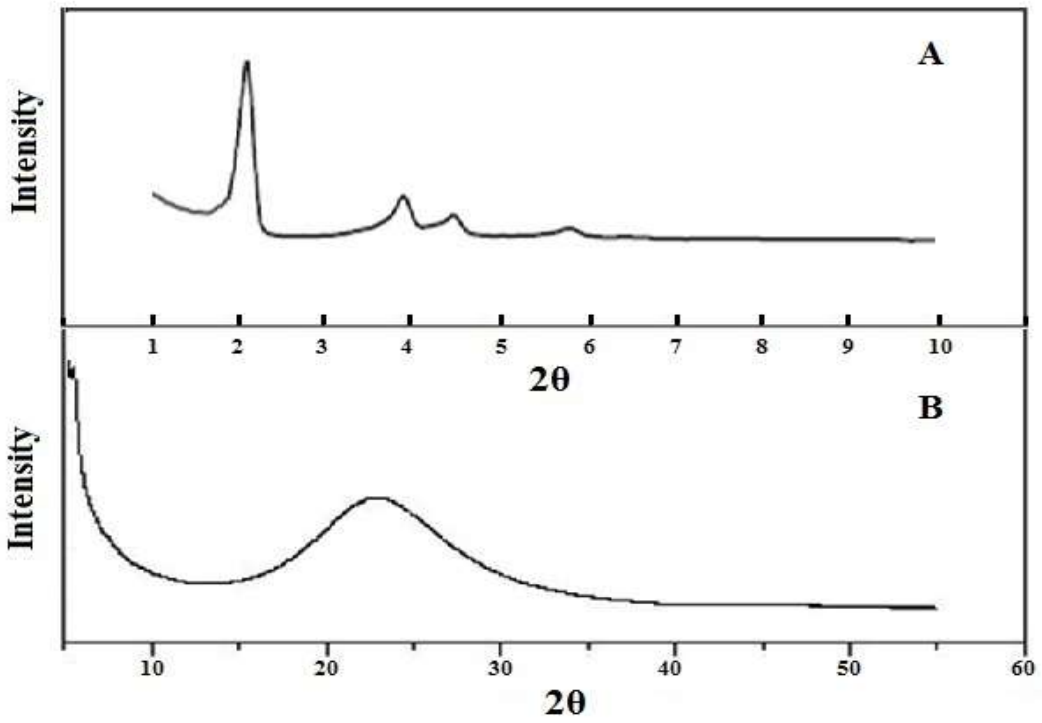

Figure 4.13: X-Ray diffraction pattern: SAXS of MSNs (A) and WAXS of MSNs (B).

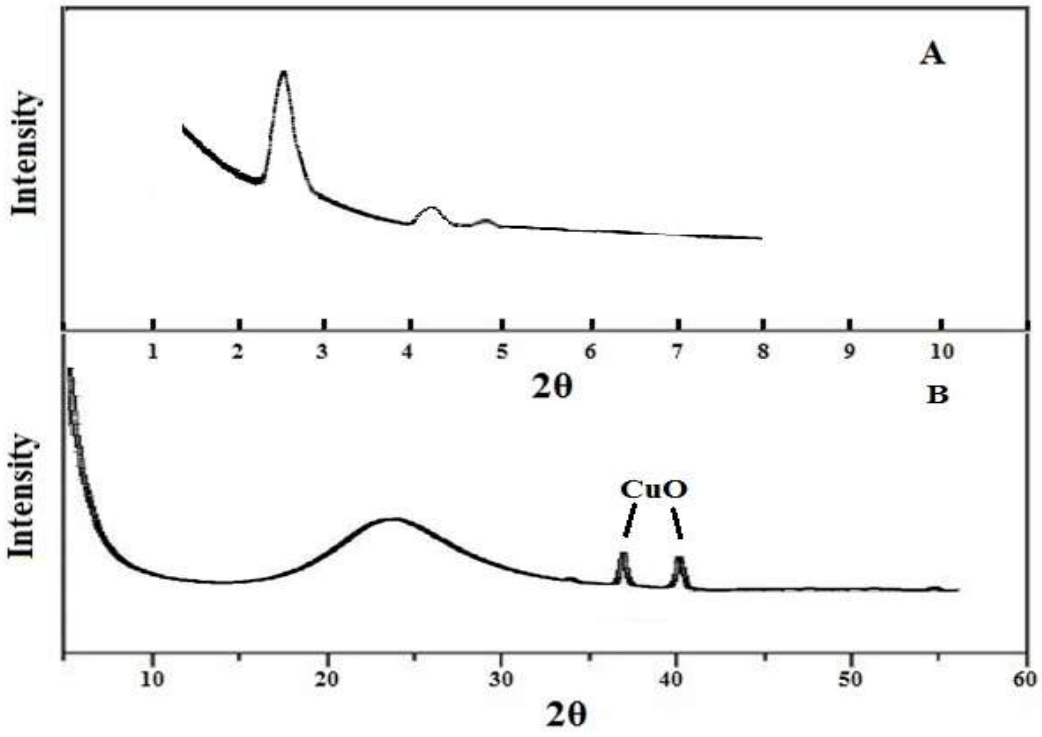

Figure 4.14: X-Ray diffraction pattern: SAXS of CuO-MSNs (A) and WAXS of MSNs (B).

- **Comparison of batch F2 with MCM-41 type of MSNs synthesized using alkoxide:**

At the end of the characterization, MCM-41 type of MSNs synthesized using commercial sodium silicate were compared with the MCM-41 type of MSNs synthesized using most frequently used silica source, TEOS, with a view to measure any significant difference observed in the MSNs synthesized using different silica precursors. Furthermore, the comparison was also made to check the extent at which commercial sodium silicate made MSNs economic.

Table 4.14: Comparison of MSNs synthesized using silicate with that of synthesized using alkoxide.

Sr. No.	Parameters	Batch F2	MSNs using alkoxide
1	Silica precursor	Commercial sodium silicate	TEOS
2	Cost of silica precursor	10 rs/litre	3825.25 rs/litre
3	Yield each ml of silica precursor produce	Approx. 1 gm	Approx. 0.2 gm
4	Particle size of MSNs	Approx. 100 nm (113 nm)	Approx. 100 nm (101 nm)
5	Surface area	850 m^2/g	934 m^2/g
6	Pore volume	1.07 $cm^3 g^{-1}$	0.81 $cm^3 g^{-1}$
7	Pore size	2.5 nm	2.9 nm

As seen in table 4.14, no significant difference was observed in the particles size or BET parameters of MSNs synthesized using two different silica precursors. Though the MSNs synthesized were comparable to each other, there was a huge difference in the price of commercial sodium silicate and TEOS. Furthermore, each ml of sodium silicate can yield

about 1 gm of MSNs whereas 5 ml of TEOS was required to yield about 1 gm of MSNs. This difference further increases the gap between the price of both silica sources.

- **Comparison of batch F2 with MCM-41 type of MSNs available in market:**

To check whether the MSNs synthesized using an economic silica source, commercial sodium silicate, were having any potential for market application, they were compared with the MCM-41 type of MSNs offered by reputed multinational companies.

Table 4.15: Comparison of batch F2 with MCM-41 type of MSNs available in market.

Sr. No.	Parameters	Batch F2	Sigma Aldrich	ACS materials
1	Colour	White	White	White
2	Form	Powder	Powder	Powder
3	Density (g/ml)	0.31	0.34	-
4	Particle size (nm)	Approx. 100	-	100-1000
5	Surface area (m^2/g)	850	Approx 1000	> 850
6	Pore volume ($cm^3 g^{-1)}$	1.07	0.98	≥ 0.75
7	Pore size (nm)	2.5	2.1-2.7	3.4

As seen in table 4.15, the MSNs synthesized using commercial sodium silicate as a silica source were comparable to MCM-41 type of MSNs offered by well known multinational companies and hence, it can be said that the synthesized MSNs have the potential to reach the market.

References:

1. Ortiz HIM, Silva AM, Cerda LAG, Castruita G, Mercado YAP. Hydrothermal Synthesis of Mesoporous Silica MCM-41 Using Commercial Sodium Silicate. Journal of the Mexican Chemical Society. 2013, 57(2):73-79.
2. Sankar R, Maheswari R, Karthik S, Shivashangari KS, Ravikumar V. Anticancer activity of Ficus religiosa engineered copper oxide nanoparticles. Material Science and Engineering C. 2014, 44:234-239.
3. Nagajyothia PC, Muthuramanb P, Sreekanthc TVM, Kim DH, Shima J. Green synthesis: In-vitro anticancer activity of copper oxide nanoparticles against human cervical carcinoma cells. Arabian Journal of Chemistry. 2017, 10(2):215-225.
4. Laha D, Pramanik A, Chattopadhyay S, Dash SK, Roy S, Pramanik P, Karmakar P. Folic acid modified copper oxide nanoparticles for targeted delivery in *in-vitro* and *in-vivo* systems. RSC Advances. 2015, 5:68169-68178.
5. Mandal AK. Copper Nanomaterials as Drug Delivery System against Infectious Agents and Cancerous Cells. Journal of Applied Life Sciences International. 2017, 15(4):1-8.
6. Bisht G, Rayamajhi S. ZnO Nanoparticles: A Promising Anticancer Agent. Nanobiomedicine. 2016, 3(9):1-11.
7. Shen C, James SA, de Jonge MD, Turney TW, Wright PF, Feltis BN. Relating cytotoxicity, zinc ions, and reactive oxygen in ZnO nanoparticle-exposed human immune cells. Toxicological Sciences. 2013, 136(1):120-30.
8. Huo C, Ouyang J, Yang H. CuO nanoparticles encapsulated inside Al-MCM-41 mesoporous materials via direct synthetic route. Scientific Reports. 2014, 4:3682.
9. Daryasari MP, Akhgar MR, Mamashli F, Bigdeli B, Khoobi M. Chitosan-folate coated mesoporous silica nanoparticles as a smart and pH-sensitive system for curcumin delivery. RSC Advances. 2016, 6:105578-105588.
10. Duo Y, Li Y, Chen C, Liu B, Wang X, Zeng X, Chen H. DOX-loaded pH-sensitive mesoporous silica nanoparticles coated with PDA and PEG induce pro-death autophagy in breast cancer. RSC Advances. 2017, 7:39641-39650.
11. Gaumet M, Vargas A, Gurny R, Delie F. Nanoparticles for drug delivery: The need for precision in reporting particle size parameters. European Journal of Pharmaceutics and Biopharmaceutics. 2008, 69:1-9.

12. Storti F, Balsamo F. Particle size distributions by laser diffraction: sensitivity of granular matter strength to analytical operating procedures. Solid Earth. 2010, 1:25-48.
13. http://www.malvern.com/en/products/product-range/zetasizer-range/zetasizer-nano-range/zetasizer-nanozs/.
14. Salopek B, Krasic D, Filipovic S. Measurement and application of zeta-potential. Zagreb. 1992, 4:147-151.
15. Collett BM. Scanning electron microscopy: a review and report of research in wood science.113-133
16. Brydson R, Brown A, Benning LG. Analytical transmission electron microscopy. Reviews in Mineralogy & Geochemistry. 2013, 78:6-51.
17. Harris PJF. Transmission Electron Microscopy of Carbon: A Brief History. Journal of Carbon Research. 2018, 4(4):1-17.
18. Hettler S, Dries M, Zeelen J, Oster M, Schroder RR, Gerthsen D. High-resolution transmission electron microscopy with an electrostatic Zach phase plate. New Journal of Physics. 2016, 18:053005.
19. Walton KS, Snurr RQ. Applicability of the BET Method for Determining Surface Areas of Microporous Metal-Organic Frameworks. Journal of the American Chemical Society. 2007, 129:8552-8556.
20. Huang X, Young NP, Townley HE. Characterization and comparison of mesoporous silica particles for optimized drug delivery. Nanomaterials and Nanotechnology. 2014, 4(2):1-15.
21. Bunaciu AA, Udriştioiu EG, Aboul-Enein HY. X-Ray Diffraction: Instrumentation and Applications. Critical Reviews in Analytical Chemistry. 2015, 45(4):289-299.
22. Olea-Mejia O, Contreras-Bulnes R, Zamudio- Ortega CM, Morales-Luckie RA, Olea-Cardoso O, Lopez-Castanares R. Scanning Electron Microscopy and Energy Dispersive Spectroscopy microanalysis applied to human dental specimens under laser irradiation for caries prevention. Microscopy: advances in scientific research and education. 2014, 70-77.
23. Newbury NE, Ritchie NWM. Is Scanning Electron Microscopy/Energy Dispersive X-ray Spectrometry (SEM/EDS) Quantitative? Scanning. 2013, 35:141-168.

24. Walsh A. The application of atomic absorption spectra to chemical analysis. Spectrochimica Acta. 1955, 7:108-117.
25. Russell BJ, Shelton JP, Walsh A. An atomic-absorption spectrophotometer and its application to the analysis of solutions. Spectrochimica Acta. 1957, 8:319-328.
26. Allan JE. Atomic-absorption spectrophotometry with special reference to the determination of magnesium. Analyst. 1958, 83:466-471.
27. David DJ. Determination of zinc and other elements in plants by atomic-absorption spectroscopy. Analyst. 1958, 83:655-661.
28. Abdalla AME, Xiao L, Ullah MW, Yu M, Ouyang C, Yang G. Current Challenges of Cancer Anti-angiogenic Therapy and the Promise of Nanotherapeutics. Theranostics. 2018, 8(2):533-548.
29. Sanaeimehr Z, Javedi I, Namvar F. Antiangiogenic and antiapoptotic effects of green‐synthesized zinc oxide nanoparticles using Sargassum muticum algae extraction. Cancer Nanotechnology. 2018, 9(3):1-16.
30. Richardson M, Singh G. Observations on the use of the avian chorioallantoic membrane (CAM) model in investigations into angiogenesis. Current Drug Targets - Cardiovascular & Hematological Disorders. 2003, 3:155–185.
31. Deryugina EI, Quigley JP. Chick embryo chorioallantoic membrane model systems to study and visualize human tumor cell metastasis. Histochemistry and Cell Biology. 2008, 130:1119–1130.
32. Tufan AC, Satiroglu-Tufan NL. The chick embryo chorioallantoic membrane as a model system for the study of tumor angiogenesis, invasion and development of anti-angiogenic agents. Current Cancer Drug Targets 2005, 5:249–266.
33. Ossowski L. In vivo invasion of modified chorioallantoic membrane by tumor cells: The role of cell surface-bound urokinase. Journal of Cell Biology. 1988, 107:2437–2445.
34. Cimpean AM, Ribatti D, Raica M. The chick embryo chorioallantoic membrane as a model to study tumor metastasis. Angiogenesis. 2008, 11:311–319.
35. Lokman NA, Elder AS, Ricciardelli C, Oehler MK. Chick Chorioallantoic Membrane (CAM) Assay as an In Vivo Model to Study the Effect of Newly Identified Molecules on Ovarian Cancer Invasion and Metastasis. International Journal of Molecular Sciences. 2008, 13(8):9959-9970.